CHEMISTRY
A European Journal

Supporting Information

Iodinated Metallacrowns: Toward Combined Bimodal Near-Infrared and X-Ray Contrast Imaging Agents

Jacob C. Lutter,[a] Svetlana V. Eliseeva,*[b] Guillaume Collet,[b] Ivana Martinić,[b] Jeff W. Kampf,[a] Bernadette L. Schneider,[a] Aidan Carichner,[a] Julien Sobilo,[c] Stéphanie Lerondel,[c] Stéphane Petoud,*[b] and Vincent L. Pecoraro*[a]

chem_201905241_sm_miscellaneous_information.pdf

Supporting Information

Table of contents

Materials

Gallium(III) nitrate hydrate (Acros, 99.9998%), samarium(III) nitrate hexahydrate (Sigma Aldrich, 99.9%), gadolinium(III) nitrate hexahydrate (Alfa, Aesar, 99.9%), ytterbium(III) nitrate pentahydrate (Sigma Aldrich, 99.9%), yttrium(III) nitrate hexahydrate (Sigma Aldrich, 99.8%), 5-iodosalicylic acid (Acros, 97%), 5-aminoisophthalic acid hydrate (Chem Impex, 99%), isophthalic acid (Acros, 99%), potassium iodide (Acros, 99%), sodium nitrite (Sigma Aldrich, 97%), sodium hydroxide (Fisher, ACS Grade), potassium hydroxide (Fisher, 85%), hydroxylamine hydrochloride (Sigma Aldrich, 99%), methanol (Fisher, ACS grade), ethanol (Decon Labs, 200 Proof), dichloromethane (Fisher, ACS Grade), ethyl acetate (Fisher, ACS Grade), sulfuric acid (Fisher, ACS Grade), hydrochloric acid (Fisher, 37% w/w), anhydrous sodium sulfate (Fisher, ACS Grade). All materials were used as received without further purification.

Synthetic Procedures

Ethyl 5-iodosalicylate. Ethyl 5-iodosalicylate was synthesized using a standard Fischer esterification.[1] Fifty mmol of 5-iodosaylicylic acid (13.20 g, 1 equiv.) was dissolved in 150 mL of 200 proof ethanol, followed by sodium sulfate such that there was an apparent reaction volume of 200 mL. Forty mmol of sulfuric acid (2.132 mL, 0.8 equiv.) were added and the reaction was warmed to reflux and stirred for 24 hours. The reaction was removed from heat and quickly vacuumed filtered to remove sodium sulfate. The clear and colorless filtrate was reduced to a volume of 30 mL using a flash evaporator. This concentrate was taken up in 50 mL of distilled water and the pH was adjusted to 8 using saturated aqueous sodium carbonate. A colorless precipitate of ethyl 5-iodosalicylate was observed and vacuum filtered from a clear and colorless filtrate. The synthetic yield was 53%. Elemental analysis for $C_9H_9IO_3$ [292.07 g/mol] % found (calculated): C 37.03 (37.01); H 2.95 (3.11). ^{1}H-NMR (400 MHz, d_6-DMSO): 10.56 ppm (1H, broad s), 8.00 ppm (1H, d), 7.78 ppm (1H, dd), 6.83 ppm (1H, d), 4.34 ppm (2H, q), 1.33 ppm (3H, t).

5-iodosalicylhydroxamic acid (H_3mishi). Fifteen mmol of ethyl 5-iodosalicylate (4.38 g, 1 equiv.) was dissolved in 75 mL of methanol to a clear and colorless solution. Separately, 45 mmol of hydroxylamine hydrochloride (3.13 g, 3 equiv.) and 60 mmol of potassium hydroxide (3.96 g, 4 equiv.) were dissolved in 75 mL of methanol to form clear and colorless solutions.

The hydroxylamine hydrochloride and potassium hydroxide solutions were combined and a colorless potassium chloride precipitate was observed. The mixture was allowed to stir for 10 minutes, then potassium chloride was vacuum filtered from a clear and colorless filtrate. This filtrate was combined with the solution of ethyl 5-iodosalicylate to form a clear and faintly yellow solution. This solution was stirred for 20 hours. Next, another set of hydroxylamine hydrochloride and potassium hydroxide solutions in 75 mL of methanol were prepared, combined and filtered as described previously to obtain another clear and colorless filtrate. This filtrate was combined into the reaction solution and let stir for another 25 hours. The resulting clear and yellow solution was then reduced to 75 mL on a flash evaporator. The concentrate was acidified to pH 1 using aqueous 2 M hydrochloric acid and then mixed into 300 mL of distilled water. An off-white precipitate formed and was vacuum filtered from a clear and yellow filtrate. The precipitate was triturated in 50 mL of dichloromethane for 20 minutes, then vacuum filtered to yield an off-white 5-iodosalicylhydroxamic acid precipitate from a faintly yellow filtrate. The synthetic yield was 89%. Elemental Analysis of $C_7H_3NO_3I$ [fw = 279.03 g/mol] found % (calculated): C, 29.94 (30.13), H, 2.10 (2.17), N, 4.96 (5.02). ^{1}H-NMR (400 MHz, *d*$_6$-DMSO): 12.17 ppm (1H, s), 11.37 ppm (1H, s), 9.39 ppm (1H, s), 7.98 ppm (1H, d), 7.65 ppm (1H, dd), 6.75 ppm (1H, d).

.

5-iodoisophthalic acid (H_2*iiph).* The preparation of 5-iodoisophthalic acid was performed by modifying a previously reported procedure.[2] Twenty-five mmol of 5-aminoisophthalic acid (4.98 g, 1 equiv.) was suspended in a mixture of 50 mL of distilled water and 50 mL of 37% hydrochloric acid to form a cloudy and pink solution. This was cooled in an ice bath and stirred. Next, 26.25 mmol of sodium nitrite (1.8113 g, 1.05 equiv.) was dissolved in 10 mL of distilled water to form a clear and colorless solution which was added to the reaction solution dropwise at a rate of 1 drop every 2 seconds. The solution became cloudy and yellow and was let stir on ice for another 10 minutes after all of the sodium nitrite was added. Then 81.25 mmol of potassium iodide (13.49 g, 3.25 equiv.) was dissolved in 40 mL of distilled water to form a clear and colorless solution which was added dropwise to the reaction at a rate of 1 drop every second. The reaction solution turned to a dark shade of purple and a brown foam formed. Once all of the potassium iodide solution was added the reaction was let warm to room temperature then warmed to about 90^{o}C as purple haze is observed. The reaction was stirred for 2.5 hours, then cooled overnight in a 4^{o}C fridge. A gray precipitate was vacuum filtered from a clear and red filtrate. This precipitate was suspended in 50 mL of methanol and warmed to reflux to form a clear and orange solution. The solution was concentrated to 20 mL under a stream of nitrogen,

then taken up in 100 mL of distilled water. The cloudy orange mixture was extracted with four 40 mL portions of ethyl acetate, dried over sodium sulfate and then filtered. The filtrate was condensed to an orange powder on a flash evaporator. This powder was triturated in 60 mL of hexane for 20 minutes, then vacuum filtered from a purple filtrate and washed with hexane until the wash fraction was no longer purple. The synthetic yield was 54% and the product was 95% pure by elemental analysis, with 5% of the 5-aminoisophthalate starting material [0.95 $C_8H_5IO_4$:0.05 $C_8H_7NO_4$]·0.75 H_2O [fw = 300.00 g/mol] % found (calculated): C 32.19 (32.03); H 2.23 (2.22); N 0.24 (0.23). ^{1}H-NMR (400 MHz, d_6-DMSO): 8.42 ppm (3H, s).

General procedure for {Ln[12-MC$_{Ga}^{III}$$_{N(L)}$-4]Na}$_2(L')_4$. 0.125 mmol of $Ln(NO_3)_3 \cdot xH_2O$ (1 equiv., Ln = Sm, Gd, Yb, Y) and 0.5 mmol of $Ga(NO_3)_3$ (0.1279 g, 4 equiv.) were dissolved in 2.5 mL of *N*,*N*-dimethylformamide (DMF) to form a clear and colorless solution. Separately, 0.5 mmol of L (4 equiv., L = H_3shi or H_3mishi) and 0.25 mmol of L' (2 equiv, L' = H_2iph or H_2iiph) was dissolved in 7.5 mL of DMF to form a clear and yellow solution. 2.0 mmol of NaOH was added as a saturated aqueous solution (101.4 μL, 16 equiv.) to the L/L' solution which forms a small amount of clear and colorless precipitate. The Ln/Ga solution was immediately added to the L/L' solution and stirred for about one hour. The solution was then gravity filtered, and the filtrate was left to crystallize in a humid environment for 2-4 weeks, yielding crystalline needles or plates.

$Sm_2Ga_8(shi)_8(iph)_4Na_2(DMF)_{12}(H_2O)_2$, **Sm-I$_0$.** The same procedure was used as above. The percent yield was 12% based on samarium nitrate hexahydrate. Elemental analysis of $Sm_2Ga_8Na_2C_{124}H_{136}N_{20}O_{54}$ [fw = 3675.02 g/mol] found % (calculated): C, 40.56 (40.53); H, 3.80 (3.73); N, 7.42 (7.62). ESI-MS, calculated $Sm_2Ga_8C_{88}H_{48}N_8O_{40}$ $[M]^{2-}$: 1359.72, found 1358.72. ^{1}H-NMR (500 MHz, d_4-MeOH): 8.66 ppm (d, 2H); 8.13 ppm (m, 2H); 7.55 ppm (t, 1H); 7.26 ppm (t, 2H); 7.05 ppm (d, 2H); 6.79 ppm (t, 2H); 5.02 ppm (s, 1H).

$Gd_2Ga_8(shi)_8(iph)_4Na_2(DMF)_{11}(H_2O)_4$, **Gd-I$_0$.** The same procedure was used as above. The percent yield was 12% based on gadolinium nitrate hexahydrate. Elemental analysis of $Gd_2Ga_8Na_2C_{121}H_{133}N_{19}O_{55}$ [fw = 3651.74 g/mol] found % (calculated): C, 39.71 (39.80); H, 3.69 (3.67); N, 7.19 (7.29). ESI-MS, calculated $Gd_2Ga_8C_{88}H_{48}N_8O_{40}$ $[M]^{2-}$: 1365.73, found 1364.72.

$Yb_2Ga_8(shi)_8(iph)_4Na_2(DMF)_{10}(H_2O)_4$, **Yb-I$_0$.** The same procedure was used as above. The percent yield was 5% based on ytterbium nitrate pentahydrate. Elemental analysis of $Yb_2Ga_8Na_2C_{118}H_{126}N_{18}O_{54}$ [fw = 3609.03 g/mol] found % (calculated): C, 39.25 (39.26); H,

3.52 (3.52); N, 7.05 (6.98). ESI-MS, calculated $Yb_2Ga_8C_{88}H_{48}N_8O_{40}$ $[M]^{2-}$: 1379.74, found 1380.74.

$Y_2Ga_8(shi)_8(iph)_4Na_2(DMF)_{10}(H_2O)_5$, **Y-I$_0$.** The same procedure was used as above. The percent yield was 13% based on yttrium nitrate hexahydrate. Elemental analysis of $Y_2Ga_8Na_2C_{121}H_{133}N_{19}O_{55}$ [fw = 3459.97 g/mol] found % (calculated): C, 41.03 (40.96); H, 3.69 (3.73); N, 7.32 (7.29). ESI-MS, calculated $Y_2Ga_8C_{88}H_{48}N_8O_{40}$ $[M]^{2-}$: 1295.71, found 1296.72. ^{1}H-NMR (500 MHz, d$_4$-MeOH): 9.10 ppm (s, 1H); 8.25 ppm (d, 2H); 8.08 ppm (d, 2H); 7.30 ppm (t, 1H); 7.26 ppm (t, 2H); 7.00 ppm (d, 2H); 6.78 ppm (t, 2H).

$Sm_2Ga_8(shi)_8(iiph)_4Na_2(DMF)_{11}(H_2O)_4$, **Sm-I$_4$.** The same procedure was used as above. The percent yield was 25% based on samarium nitrate hexahydrate. Elemental analysis of $Sm_2Ga_8Na_2C_{121}H_{129}N_{19}O_{55}I_4$ [fw = 4141.54 g/mol] found % (calculated): C, 35.34 (35.09); H, 3.11 (3.14); N, 6.46 (6.43). ESI-MS, calculated $Sm_2Ga_8C_{88}H_{44}N_8O_{40}I_4$ $[M]^{2-}$: 1611.51, found 1609.50. ^{1}H-NMR (500 MHz, *d$_4$*-MeOH): 8.92 ppm (1H, s); 8.87 ppm (0.5H, s); 8.54 ppm (0.5H, broad s); 8.15 ppm (1.5H, d); 7.51 ppm (1H, broad s); 7.27 ppm (1.5H, m); 7.05 ppm (1.5H, m); 6.80 ppm (1.5H, m); 5.10 ppm (1H, m).

$Gd_2Ga_8(shi)_8(iiph)_4Na_2(DMF)_{10}(H_2O)_5$, **Gd-I$_4$.** The same procedure was used as above. The percent yield was 22% based on gadolinium nitrate hexahydrate. Elemental analysis of $Gd_2Ga_8Na_2C_{118}H_{124}N_{18}O_{55}I_4$ [fw = 4100.24 g/mol] found % (calculated): C, 34.65 (34.57); H, 3.18 (3.05); N, 6.04 (6.15). ESI-MS, calculated $Gd_2Ga_8C_{88}H_{44}N_8O_{40}I_4$ $[M]^{2-}$: 1617.52, found 1616.51.

$Yb_2Ga_8(shi)_8(iiph)_4Na_2(DMF)_{13}(H_2O)_6$, **Yb-I$_4$.** The same procedure was used as above. The percent yield was 20% based on ytterbium nitrate pentahydrate. Elemental analysis of $Yb_2Ga_8Na_2C_{127}H_{147}N_{21}O_{59}I_4$ [fw = 4369.15 g/mol] found % (calculated): C, 34.89 (34.91); H, 3.47 (3.39); N, 6.68 (6.73). ESI-MS, calculated $Yb_2Ga_8C_{88}H_{44}N_8O_{40}I_4$ $[M]^{2-}$: 1631.53, found 1632.52.

$Y_2Ga_8(shi)_8(iiph)_4Na_2(DMF)_{12}(H_2O)_3$, **Y-I$_4$.** The same procedure was used as above. The percent yield was 28% based on yttrium nitrate hexahydrate. Elemental analysis of $Y_2Ga_8Na_2C_{124}H_{134}N_{20}O_{55}I_4$ [fw = 4073.71 g/mol] found % (calculated): C, 36.66 (36.56); H, 3.38 (3.32); N, 6.53 (6.88). ESI-MS, calculated $Y_2Ga_8C_{88}H_{44}N_8O_{40}I_4$ $[M]^{2-}$: 1547.50, found 1548.49. ^{1}H-NMR (500 MHz, *d$_4$*-MeOH): 8.99 ppm (1H, d); 8.58 ppm (0.5H, d); 8.55 ppm

(1H, s); 8.51 ppm (0.5H, s); 8.01-8.09 ppm (2H, m); 7.59 ppm (0.5H, t); 7.26 ppm (1.5H, m); 7.01 ppm (1.5H, m); 6.78 ppm (1.5H, t).

$Sm_2Ga_8(mishi)_8(iph)_4Na_2(DMF)_{14}(H_2O)_4$, **Sm-$I_8$.** The same procedure was used as above. The percent yield was 15% based on samarium nitrate hexahydrate. Elemental analysis of *$Sm_2Ga_8Na_2C_{130}H_{146}N_{22}O_{58}I_8$* [fw = 4864.41 g/mol] found % (calculated): C, 32.29 (32.10); H, 3.04 (3.03); N, 6.43 (6.33). ESI-MS, calculated *$Sm_2Ga_8C_{88}H_{40}N_8O_{40}I_8$* $[M]^{2-}$: 1863.31, found 1862.29. ^{1}H-NMR (500 MHz, *d_4*-MeOH): 8.69 ppm (2H, d); 8.62 ppm (1H, d); 8.36 ppm (2H, dd); 7.57 ppm (1H, q); 7.50 ppm (2H, d), 6.86 ppm (2H, d).

$Gd_2Ga_8(mishi)_8(iph)_4Na_2(DMF)_8(H_2O)_4$, **Gd-$I_8$.** The same procedure was used as above. The percent yield was 9% based on gadolinium nitrate hexahydrate. Elemental analysis of *$Gd_2Ga_8Na_2C_{112}H_{104}N_{16}O_{52}I_8$* [fw = 4439.62 g/mol] found % (calculated): C, 30.37 (30.30); H, 2.54 (2.36); N, 5.07 (5.05). ESI-MS, calculated *$Gd_2Ga_8C_{88}H_{40}N_8O_{40}I_8$* $[M]^{2-}$: 1869.31, found 1868.30.

$Yb_2Ga_8(mishi)_8(iph)_4Na_2(DMF)_{16}(H_2O)_8$, **Yb-$I_8$.** The same procedure was used as above. The percent yield was 24% based on ytterbium nitrate pentahydrate. Elemental analysis of *$Yb_2Ga_8Na_2C_{136}H_{168}N_{24}O_{64}I_8$* [fw = 5128.05 g/mol] found % (calculated): C, 31.91 (31.85); H, 3.33 (3.30); N, 6.45 (6.56). ESI-MS, calculated *$Yb_2Ga_8C_{88}H_{40}N_8O_{40}I_8$* $[M]^{2-}$: 1883.32, found 1884.31.

$Y_2Ga_8(mishi)_8(iph)_4Na_2(DMF)_{12}(H_2O)_4$, **Y-$I_8$.** The same procedure was used as above. The percent yield was 24% based on yttrium nitrate hexahydrate. Elemental analysis of *$Y_2Ga_8Na_2C_{124}H_{132}N_{20}O_{56}I_8$* [fw = 4595.31 g/mol] found % (calculated): C, 32.36 (32.41); H, 2.89 (2.90); N, 6.04 (6.10). ESI-MS, calculated *$Y_2Ga_8C_{88}H_{40}N_8O_{40}I_8$* $[M]^{2-}$: 1799.29, found 1800.28. 1H-NMR (500 mHz, d4-MeOH): 9.07 ppm (1H, d), 8.32 ppm (2H, m), 8.25 ppm (1H, d), 8.20 ppm (1H, d), 7.48 ppm (2H, d), 7.30 ppm (1H, q), 6.80 ppm (2H, d).

$Sm_2Ga_8(mishi)_8(iiph)_4Na_2(DMF)_{12}(H_2O)_2$, **Sm-$I_{12}$.** The same procedure was used as above. The percent yield was 32% based on samarium nitrate hexahydrate. Elemental analysis of *$Sm_2Ga_8Na_2C_{124}H_{124}N_{20}O_{54}I_{12}$* [fw = 5185.78 g/mol] found % (calculated): C, 28.76 (28.72); H, 2.46 (2.41); N, 5.36 (5.40). ESI-MS, calculated *$Sm_2Ga_8C_{88}H_{36}N_8O_{40}I_{12}$* $[M]^{2-}$: 2115.10, found 2114.08. ^{1}H-NMR (500 MHz, *d_6*-DMSO): 8.51 ppm (1H, d); 8.42 ppm (1H, s); 8.12 ppm (2 H, m); 7.46 ppm (2H, d), 6.78 ppm (2H, d), 5.41 ppm (1H, d).

$Gd_2Ga_8(mishi)_8(iiph)_4Na_2(DMF)_{16}(H_2O)_5$, **Gd-$I_{12}$.** The same procedure was used as above. The percent yield was 34% based on gadolinium nitrate hexahydrate. Elemental analysis of *$Gd_2Ga_8Na_2C_{136}H_{158}N_{24}O_{61}I_{12}$* [fw = 5545.98 g/mol] found % (calculated): C, 29.44 (29.45); H, 2.91 (2.87); N, 5.96 (6.06). ESI-MS, calculated *$Gd_2Ga_8C_{88}H_{36}N_8O_{40}I_{12}$* $[M]^{2-}$: 2121.11, found 2120.09.

$Yb_2Ga_8(mishi)_8(iiph)_4Na_2(DMF)_{14}(H_2O)_4$, **Yb-$I_{12}$.** The same procedure was used as above. The percent yield was 35% based on ytterbium nitrate pentahydrate. Elemental analysis of *$Yb_2Ga_8Na_2C_{130}H_{142}N_{22}O_{58}I_{12}$* [fw = 5413.39 g/mol] found % (calculated): C, 28.86 (28.84); H, 2.59 (2.64); N, 5.59 (5.69). ESI-MS, calculated *$Yb_2Ga_8C_{88}H_{36}N_8O_{40}I_{12}$* $[M]^{2-}$: 2135.12, found 2136.10.

$Y_2Ga_8(mishi)_8(iiph)_4Na_2(DMF)_{15}(H_2O)_5$, **Y-$I_{12}$.** The same procedure was used as above. The percent yield was 33% based on yttrium nitrate pentahydrate. Elemental analysis of *$Y_2Ga_8Na_2C_{133}H_{151}N_{23}O_{60}I_{12}$* [fw = 5336.20 g/mol] found % (calculated): C, 30.05 (29.94); H, 2.86 (2.85); N, 5.89 (6.04). ESI-MS, calculated *$Y_2Ga_8C_{88}H_{36}N_8O_{40}I_{12}$* $[M]^{2-}$: 2051.09, found 2052.08. ^{1}H-NMR (500 MHz, d_6-DMSO): 8.69 ppm (1H, d); 8.05-8.20 ppm (4H, m), 7.41 ppm (2H, d), 6.72 ppm (2H, t).

Physical Methods

Mass-spectrometry

ESI-QTOF MS was performed on an Agilent 6520 Accurate-Mass Q-TOF LC/MS quadrupole time of flight mass spectrometer in negative ion mode with a fragmentation voltage of 250 V. Samples were prepared by dissolving approximately 1 mg of compound in 1 mL of methanol, then diluting 20 μL of the solution into another 1 mL of methanol. Samples were directly injected using a syringe (without the HPLC or an autosampler). Data were processed with Agilent MassHunter Qualitative Analysis software. Elemental analysis was performed on a Carlo Erba 1108 elemental analyzer and a PerkinElmer 2400 elemental analyzer by Atlantic Microlabs, Inc.

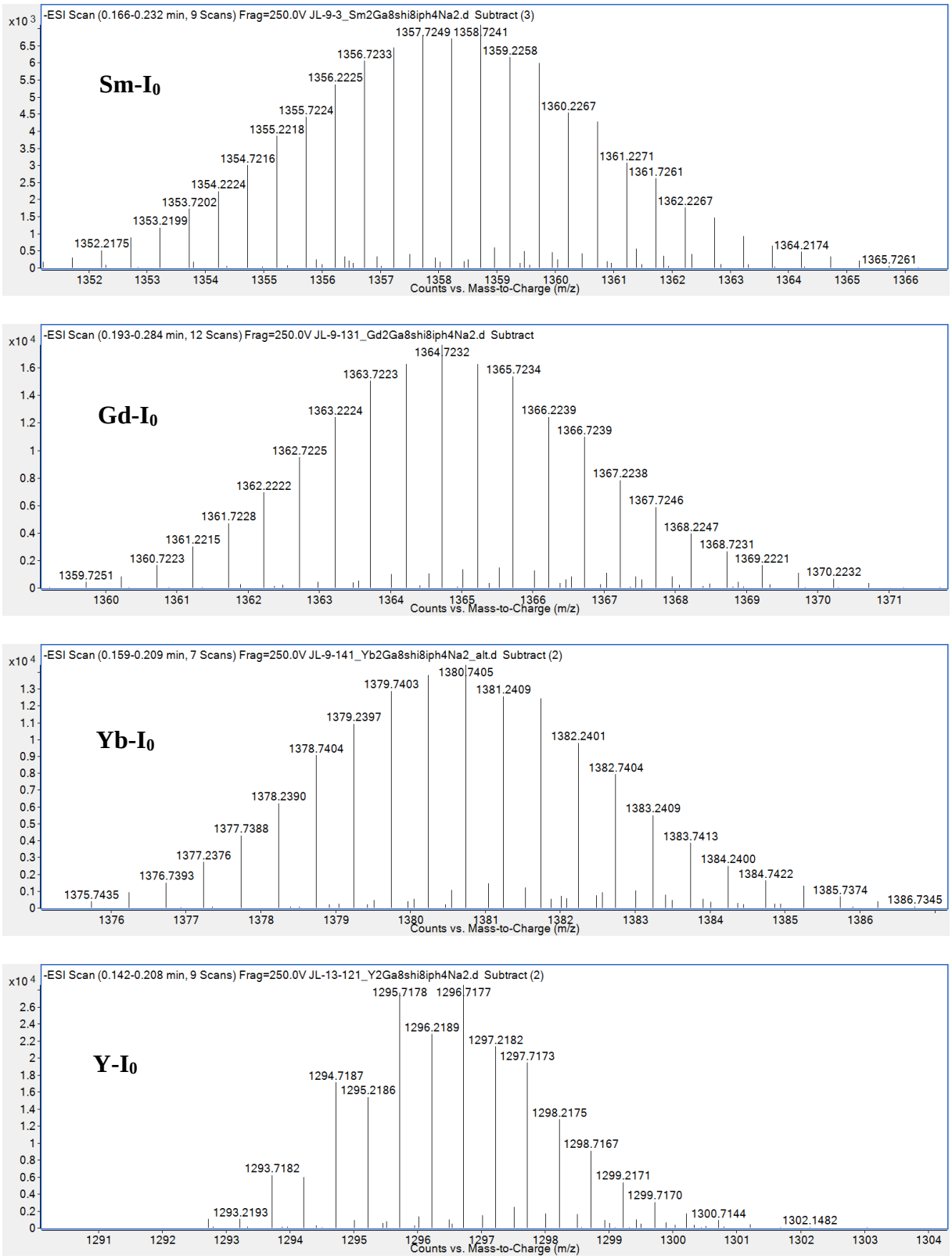

Figure S 1. Results of ESI-MS analyses performed on **Ln-I$_0$** complexes. Spectra were collected in negative ion mode with a fragmentation voltage of 250V in methanol. Background spectra were subtracted twice.

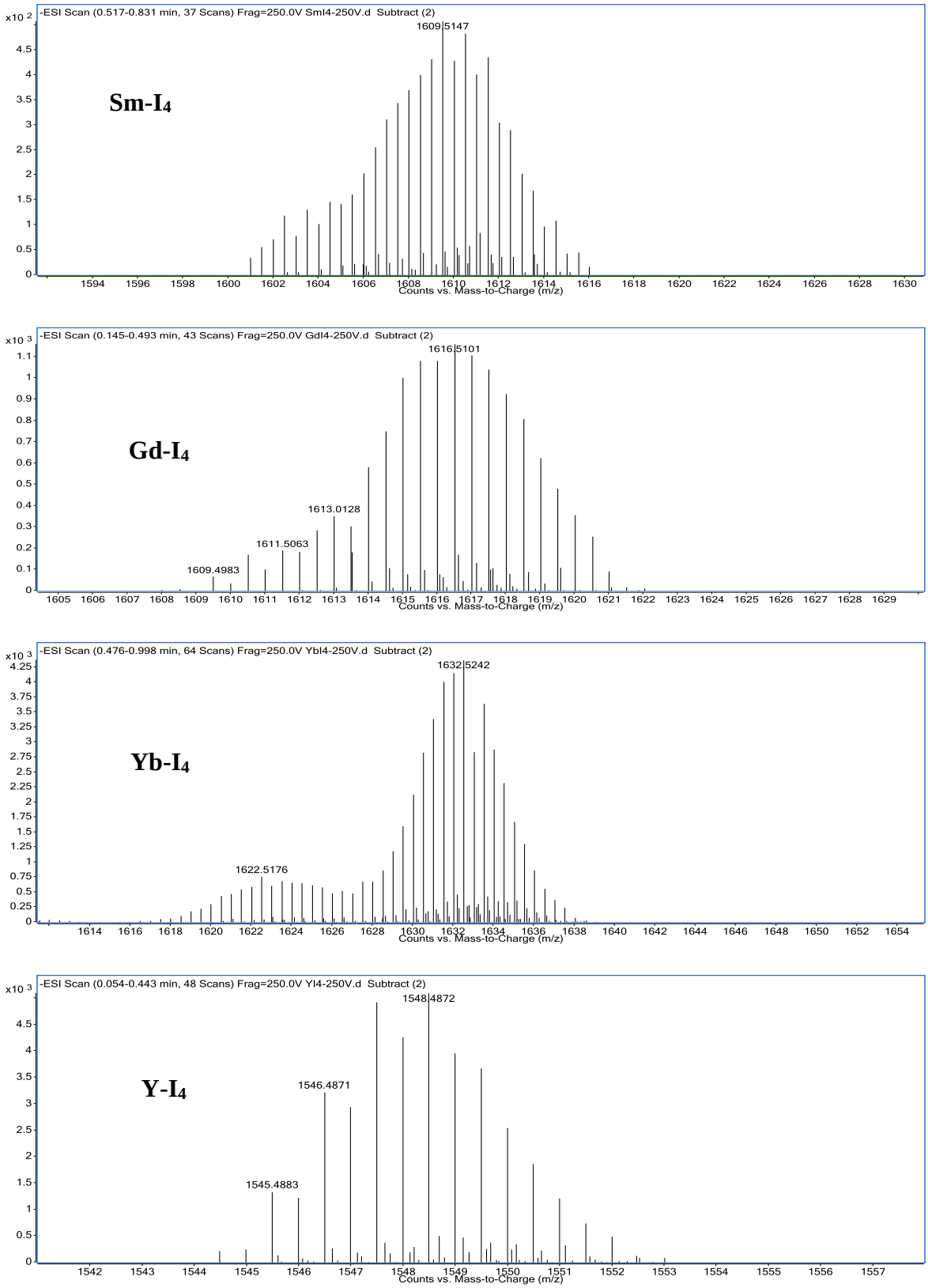

Figure S 2. Results of ESI-MS analyses performed on **Ln-I$_4$** complexes. Spectra were collected in negative ion mode with a fragmentation voltage of 250V in methanol. Background spectra were subtracted twice.

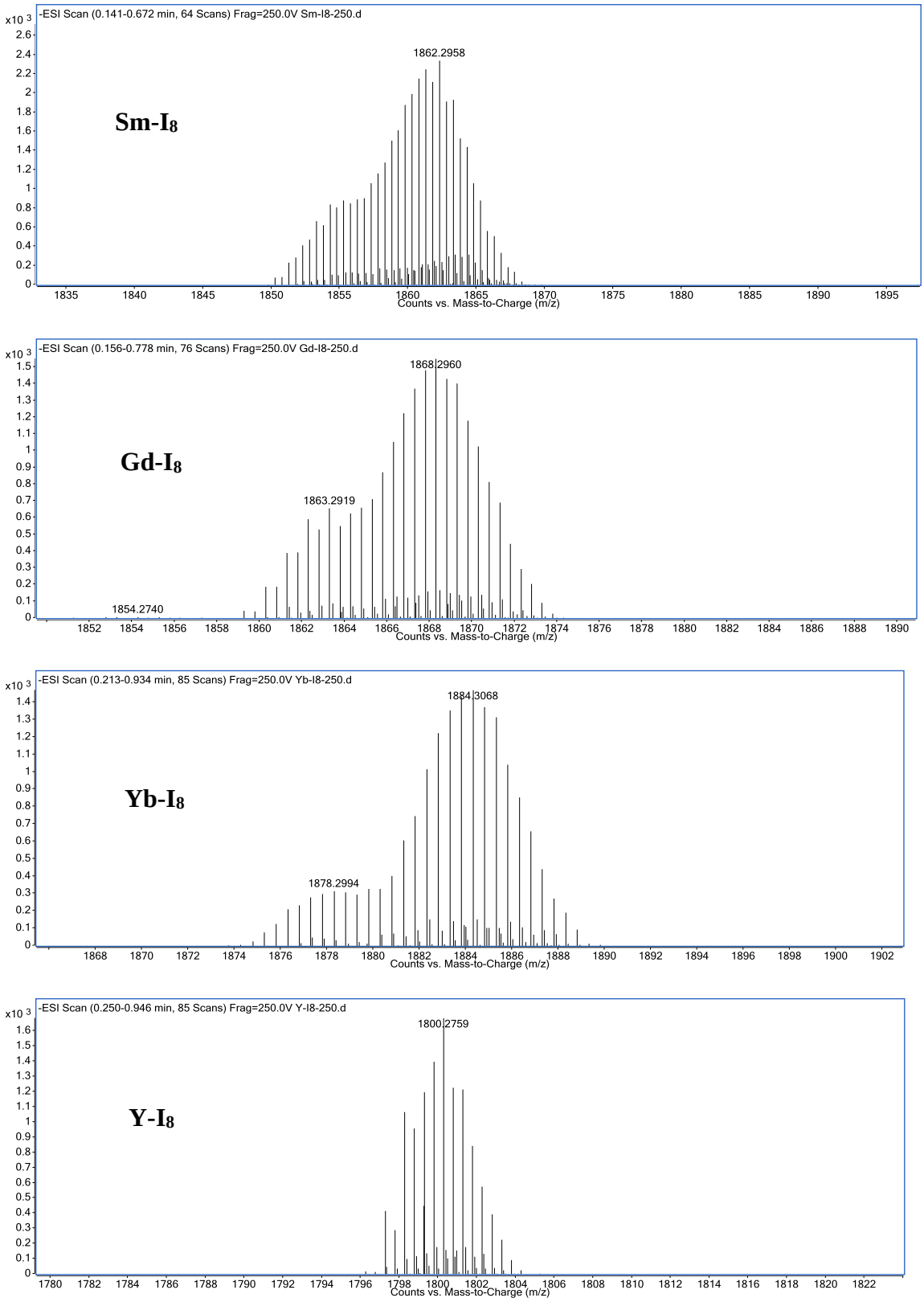

Figure S 3. Results of ESI-MS analyses performed on **Ln-I$_8$** complexes. Spectra were collected in negative ion mode with a fragmentation voltage of 250V in methanol. Background spectra were subtracted twice.

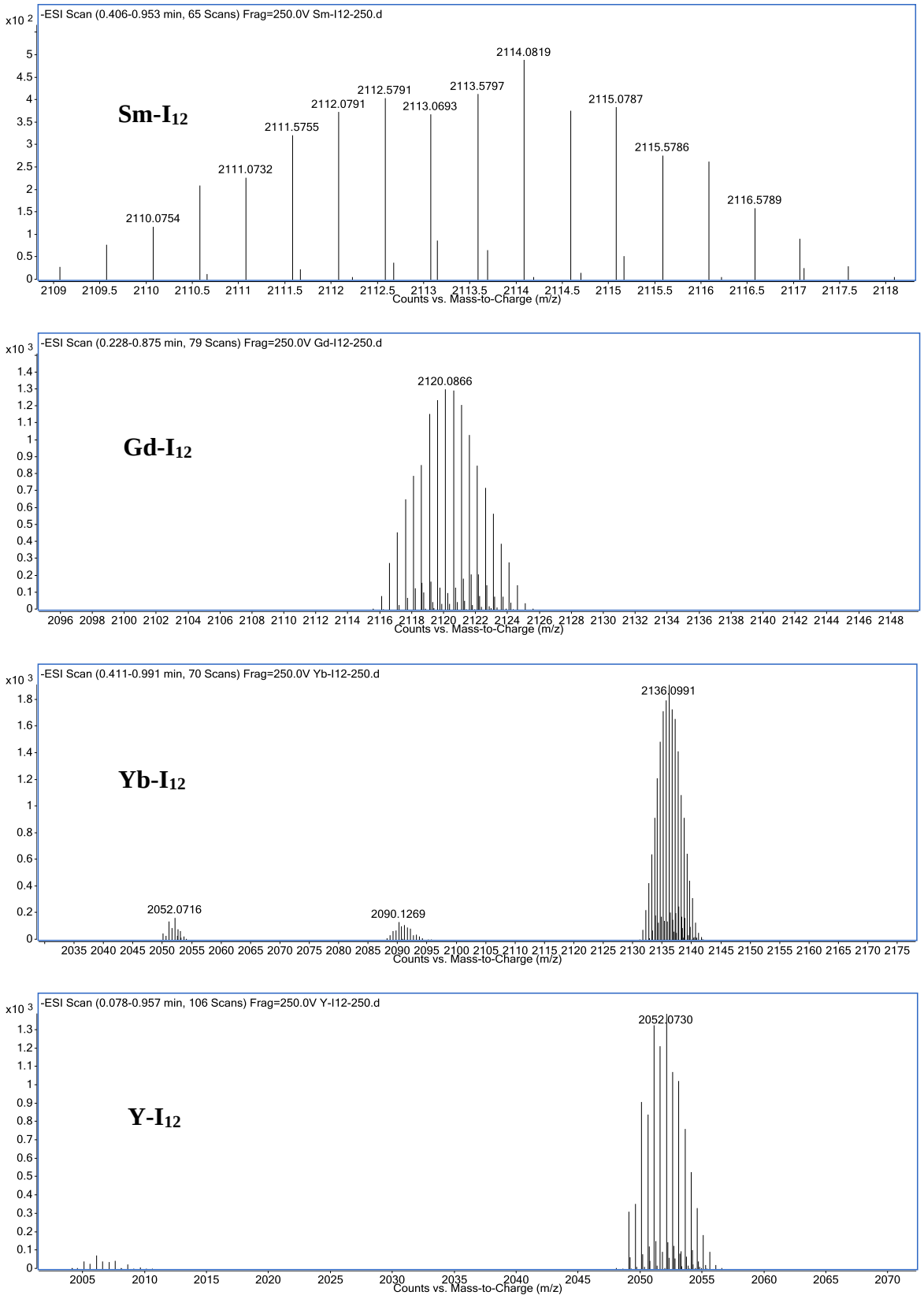

Figure S 4. Results of ESI-MS analyses performed on **Ln-I$_{12}$** complexes. Spectra were collected in negative ion mode with a fragmentation voltage of 250V in methanol. Background spectra were subtracted twice.

Proton Nuclear Magnetic Resonance

^{1}H NMR spectra were collected using a 400 MHz Varian MR400 spectrometer for organic molecules or a 500 MHz Varian VNMRS 500 spectrometer for the metallacrown complexes. Solutions were prepared in *d*$_6$-DMSO for organic molecules or *d*$_4$-MeOH for metallacrown complexes and collected using a standard pulse sequence for 45^{o} excitation. Spectra were processed using MestraNOVA 6.0 software.

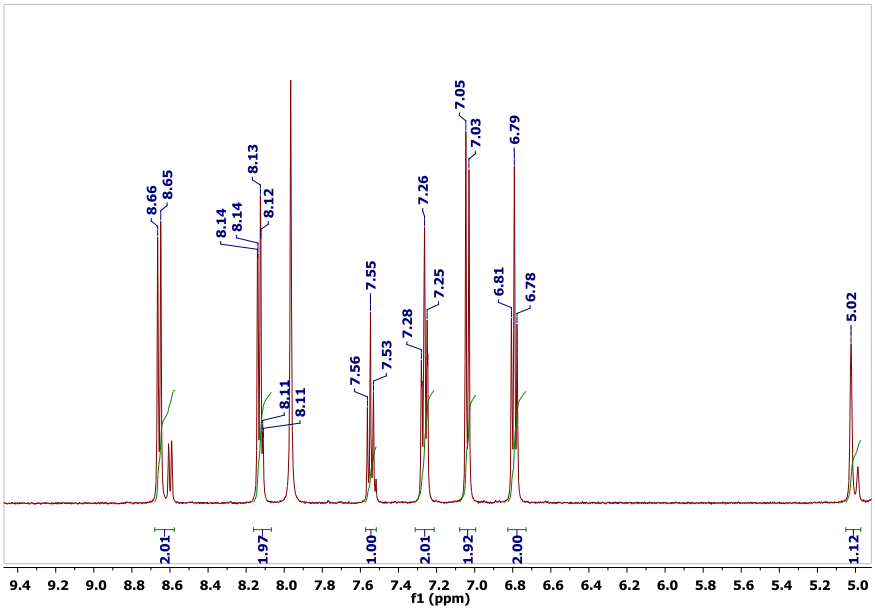

Figure S 5. ^{1}H-NMR spectrum of **Sm-I$_0$** in *d*$_4$-MeOH at room temperature.

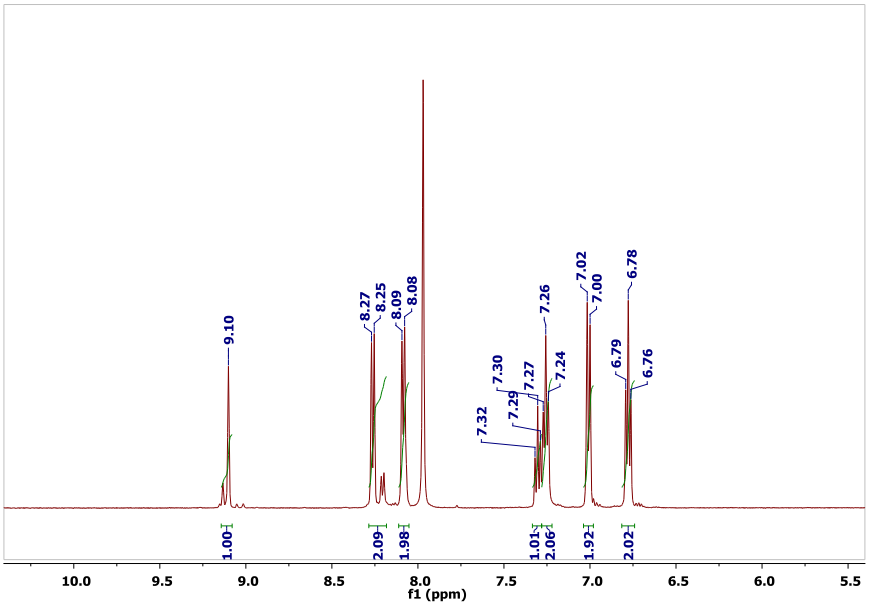

Figure S 6. ^{1}H-NMR spectrum of **Y-I$_0$** in *d*$_4$-MeOH at room temperature.

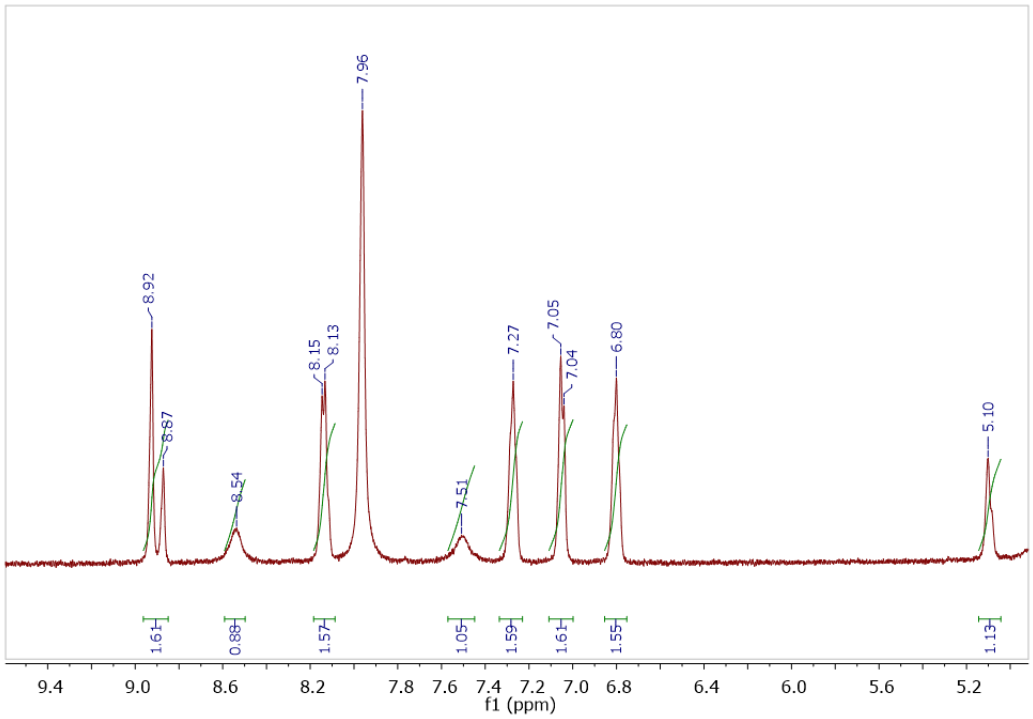

Figure S 7. ^{1}H-NMR spectrum of **Sm-I$_4$** in *d$_4$*-MeOH at room temperature.

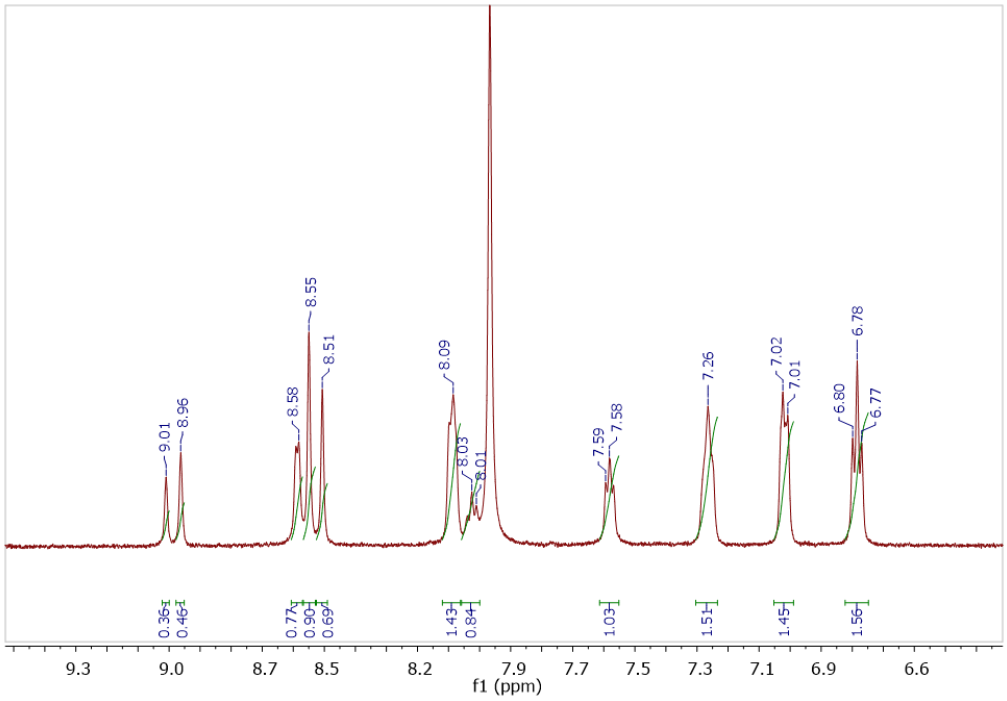

Figure S 8. ^{1}H-NMR spectrum of **Y-I$_4$** in *d$_4$*-MeOH at room temperature.

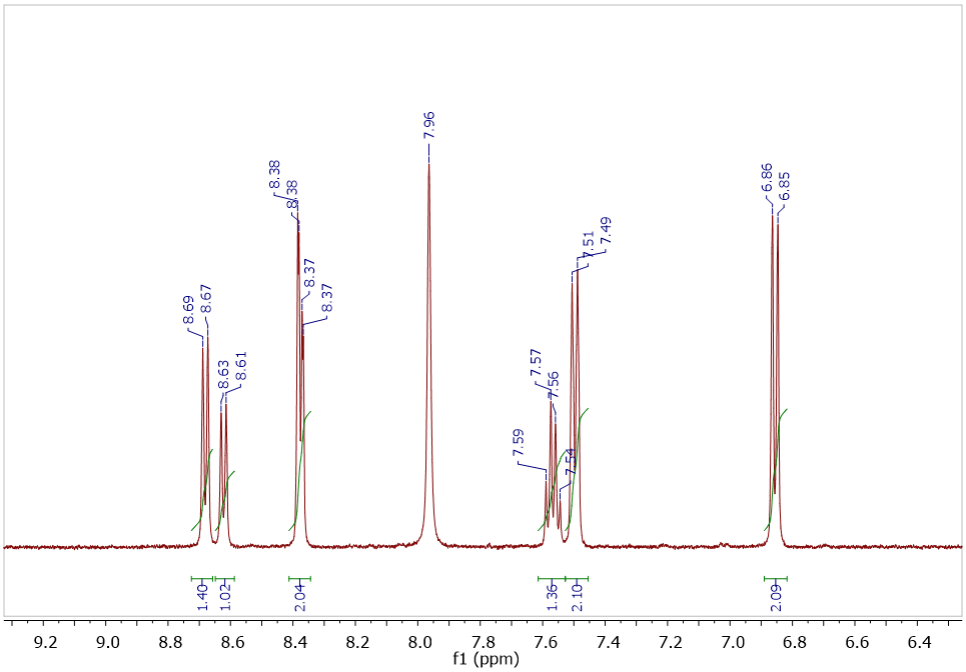

Figure S 9. ^{1}H-NMR spectrum of **Sm-I$_8$** in *d*$_4$-MeOH at room temperature.

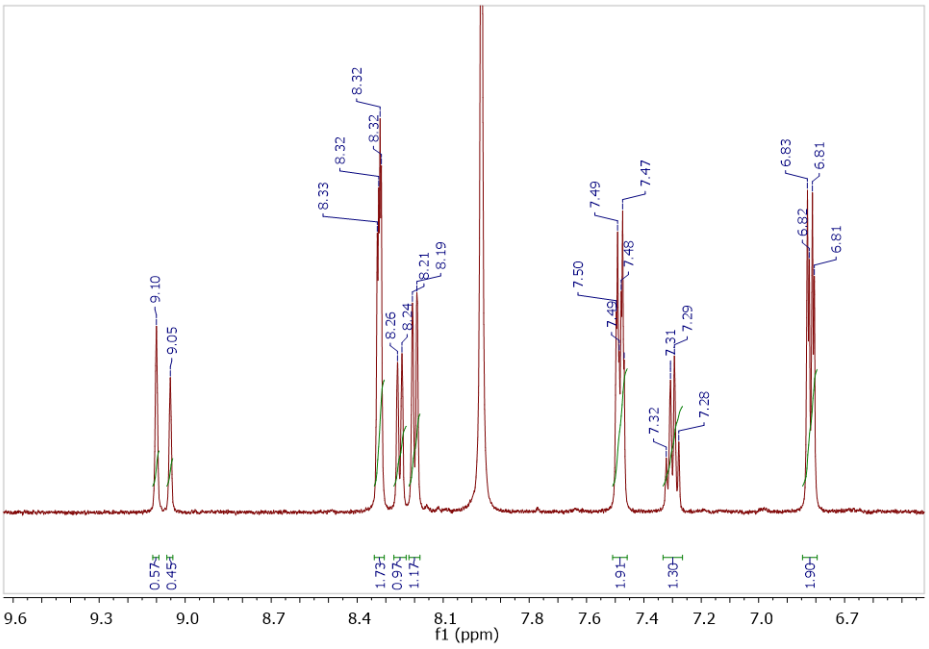

Figure S 10. ^{1}H-NMR spectrum of **Y-I$_8$** in *d*$_4$-MeOH at room temperature.

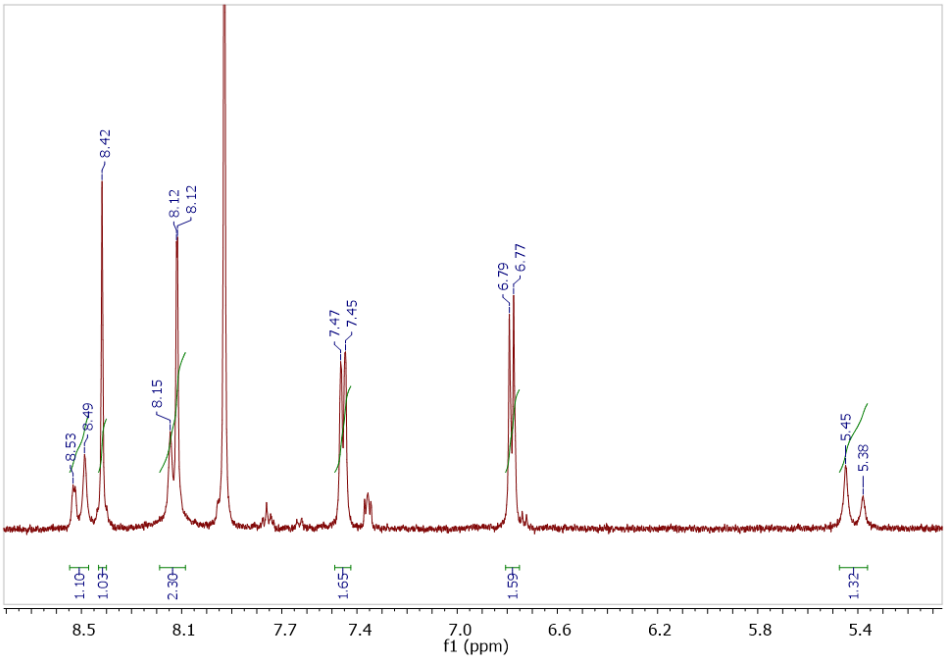

Figure S 11. ^{1}H-NMR spectrum of **Sm-I$_{12}$** in *d*$_6$-DMSO at room temperature.

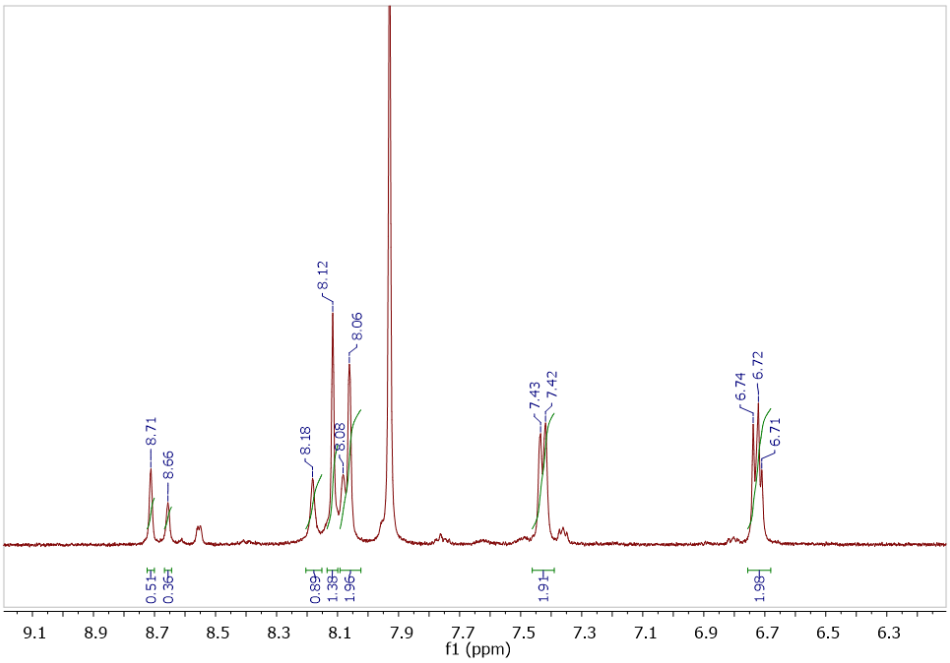

Figure S 12. ^{1}H-NMR spectrum of **Y-I$_{12}$** in *d*$_6$-DMSO at room temperature.

X-ray Crystallography

Yellow plates of **Sm-I$_4$** were grown from a dimethylformamide solution of the compound at 22 ^{o}C. A crystal of dimensions 0.13 x 0.12 x 0.09 mm was mounted on a Rigaku AFC10K Saturn 944+ CCD-based X-ray diffractometer equipped with a low temperature sample holder and Micromax-007HF Cu-target micro-focus rotating anode (λ = 1.54187 Å) operated at 1.2 kW power (40 kV, 30 mA). The X-ray intensities were measured at 85(1) K with the detector placed at a distance 42.00 mm from the crystal. A total of 2028 images were collected with an oscillation width of 1.0^o in ω. The exposure times were 1 sec. for the low angle images, 5 sec. for high angle. Rigaku d*trek images were exported to CrysAlisPro 1.171.38.41 (Rigaku Oxford Diffraction, 2015) for processing and corrected for absorption. The integration of the data yielded a total of 76333 reflections to a maximum 2θ value of 138.70^o of which 4675 were independent and 4656 were greater than 2σ(I). The final cell constants (Table S1) were based on the xyz centroids of 46786 reflections above 10σ(I). Analysis of the data showed negligible decay during data collection. The structure was solved and refined with the Bruker SHELXTL (version 2018/3) software package,[3] using the space group I4/m with Z = 2 for the formula $C_{100}H_{100}N_{12}O_{57}Na_2Ga_8Sm_2I_4$. All non-hydrogen atoms were refined anisotropically with the hydrogen atoms placed in idealized positions. The structure is disordered in two rotationally related orientations which were refined by use of partial occupancy atoms and use of restraints. Full matrix least-squares refinement based on F^2 converged at R1 = 0.0619 and wR2 = 0.1815 [based on I > 2σ(I)], R1 = 0.0620 and wR2 = 0.1816 for all data. The SQUEEZE subroutine of the PLATON program suite[4,5] was used to address the disordered solvent in the two large cavities present in the structure. Additional details are presented in Table S1 and are given as Supporting Information in a CIF file.

Colorless blocks of **Sm-I$_8$** were grown from a dimethylformamide solution of the compound at 22 ^{o}C. A crystal of dimensions 0.21 x 0.03 x 0.03 mm was mounted on a Rigaku AFC10K Saturn 944+ CCD-based X-ray diffractometer equipped with a low temperature device and Micromax-007HF Cu-target micro-focus rotating anode (λ = 1.54187 Å) operated at 1.2 kW power (40 kV, 30 mA). The X-ray intensities were measured at 85(1) K with the detector placed at a distance 42.00 mm from the crystal. A total of 2028 images were collected with an oscillation width of 1.0^o in ω. The exposure times were 1 sec. for the low angle images, 5 sec. for high angle. Rigaku d*trek images were exported to CrysAlisPro 1.171.38.41 (Rigaku Oxford Diffraction, 2015) for processing and corrected for absorption. The integration of the data yielded a total of 145338 reflections to a maximum 2θ value of 139.77^o of which 34374 were independent and 32830 were greater than 2σ(I). The final cell constants (Table S1) were

based on the xyz centroids of 62082 reflections above 10σ(I). Analysis of the data showed negligible decay during data collection. The structure was solved and refined with the Bruker SHELXTL (version 2018/3) software package,[3] using the space group $P\bar{1}$ with Z = 1 for the formula $C_{255.5}H_{297.2}N_{42.5}O_{122}Na_3Ga_{16}Sm_4I_{16}$. All non-hydrogen atoms were refined anisotropically with the hydrogen atoms placed in idealized positions. Full matrix least-squares refinement based on F^2 converged at $R_1 = 0.0530$ and $wR_2 = 0.1481$ [based on $I > 2\sigma(I)$], $R_1 = 0.0556$ and $wR_2 = 0.1527$ for all data. The SQUEEZE subroutine of the PLATON program suite[4,5] was used to address the disordered solvent in the large cavities present in the structure. Additional details are presented in Table S1 and are given as Supporting Information in a CIF file.

The **Sm-I$_4$** crystallized in I4/m and similarly to the reported $\{Ln[12\text{-}MC_{Ga^{III}N(shi)}\text{-}4]\}_2(iph)_4$ MC,[6] the two $Ln[12\text{-}MC_{Ga^{III}N(shi)}\text{-}4]$ motifs are bridged by 5-iodoisophthalate such that each Sm^{3+} is eight-coordinate with a square antiprismatic geometry (Figure S13). All Ga^{3+} are six-coordinate and octahedral with hydroximate ligands in equatorial positions, as well as a carboxylate oxygen and solvent in the axial positions. Sodium countercations are bound to the MC in a nine-coordinate monocapped square antiprism geometry on the opposite face of the MC from the Sm^{3+}. The **Sm-I$_8$** structure crystallized in $P\bar{1}$ and showed two crystallographically distinct MCs where the Na^+ binds in two different sites. The first one (Figure S14a) is the equivalent nine-coordinate monocapped square antiprism seen in **Sm-I$_4$**, whereas the second has the Na^+ bound to the side of the MC in a six coordinate octahedral environment (Figure S14b). Three atoms come from solvent molecules, while the other three are the phenolic and carbonyl oxygens of the $mishi^{3-}$ in addition to a carboxylate of the iph^{2-}.

Compositional Analysis

The reaction of stoichiometric amounts of Ln^{3+} and Ga^{3+} nitrates with H_3shi and H_2iph ligands or their iodinated derivatives in DMF in presence of NaOH yielded the generation of unprecedented dimeric MCs with Ln[12-MC-4] motifs with controlled iodide content. X-ray quality crystals were obtained for **Sm-I$_4$**, and **Sm-I$_8$** and their molecular structures are depicted in Figure 1b, c in the main text. Crystallographic analysis reveals that the bond connectivities related to the Ga(III) and Ln(III) ions of these molecules are comparable to those described previously for dimeric MCs formed with Ga(III) or Mn(III).[6,7] Some level of molecular disorder is observed due to the presence of diasteriomers formed by the combinations of clockwise (cMC) and anticlockwise (aMC) MC enantiomers paired across the isophthalate or 5-iodoisophthalate bridges.[8] Serendipitously, such disorder was not observed in the **Sm-I$_8$**

structure which crystallized in $P\bar{1}$ (Figure 1c) as opposed to I4/m for **Sm-I$_4$**; however, the analysis of **Sm-I$_8$** structure showed the presence of two crystallographically distinct MCs where the Na^+ is connected to two different sites. An overlay of crystal structures of **Ln-I$_0$** with NH_4^+, **Ln-I$_4$** and both types of **Ln-I$_8$** demonstrate minor changes in coordination geometries between the different species (Figure S13), highlighting the generalizable nature of this scaffold. Thus, a remarkable range and level of tunability and a possibility of controlled design of this family of Ln^{3+}/Ga^{3+} MCs for specific purposes can be achieved. It should be noted, however, that the previously reported $\{Ln[12\text{-}MC_{Ga^{III}N(shi)}\text{-}4]\}_2(iph)_4$ structure was obtained with NH_4^+ as countercation instead of Na^+ for the corresponding iodinated analogues. In order to eliminate contributions of the natures of counter-cations and to obtain an unambiguous comparison between the systems, we have synthesized the corresponding $\{Ln[12\text{-}MC_{Ga^{III}N(shi)}\text{-}4]\}_2(iph)_4$ with Na^+, hereafter referred to as **Ln-I$_0$**. ^{1}H-NMR, ESI-MS, (Figures S1–S12) and elemental analysis confirm that all analogues have the same stoichiometric composition in each series and differ only in the number of extraneous solvent molecules. ^{1}H-NMR spectra of **Ln-I$_4$**, **Ln-I$_8$** and **Ln-I$_{12}$** species (Ln = Y, Sm; Figures S7–S12) show the expected signals arising from salicylhydroximate and isophthalate ligands or their derivatives in a 2:1 ratio due to the pseudo 4-fold symmetry which is common for all these complexes. The presence of major and minor overlapping peaks in the ^{1}H-NMR spectra suggest the presence of clockwise and anticlockwise diastereomers of metallacrowns in solution for all the species. The stability of **Ln-I$_x$** in methanol suggested by ^{1}H-NMR is confirmed by the recording of consistent ESI-MS spectra (Figure S1–S4).

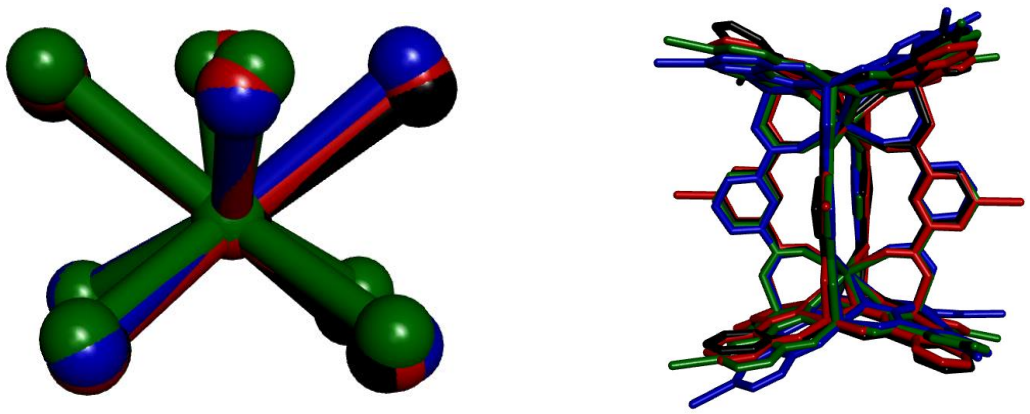

Figure S 13. Superposition of (left) first coordination spheres (square antiprism) of corresponding lanthanide(III) ions and (right) Ln_2Ga_8 structural motifs in **Dy-I$_0$** (black),[6] **Sm-I$_4$** (red), **Sm-I$_8$a** (green) and **Sm-I$_8$b** (blue).

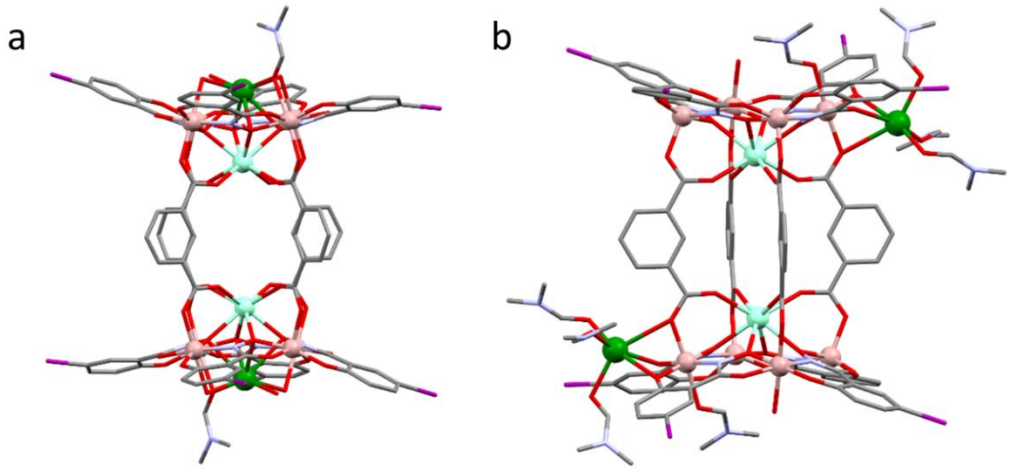

Figure S 14. X-ray crystal structures of **Sm-I$_8$** with sodium atoms bound (a) on the top and below the Ln[12-MC$_{Ga}{}^{III}{}_{N(mishi)}$-4] motifs or (b) on the sides. Sm: cyan; Ga: rose; O: red; N: light blue; C: grey; I: purple; Na: green. The hydrogen atoms and solvent molecules have been omitted for clarity.

Table S1. Crystallographic Parameters for **Sm-I$_4$** and **Sm-I$_8$**

Compound	**Sm-I$_4$**	**Sm-I$_8$**
Chemical Formula	$C_{100}H_{100}Ga_8I_4N_{12}Na_2O_{57}Sm_2$	$C_{255.5}H_{297.2}Ga_{16}I_{16}N_{42.5}Na_3O_{122}Sm_4$
Formula Weight	3993.95 g/mol	9731.83 g/mol
Crystal System, Space Group	Tetragonal, I4/m (No. 87)	Triclinic, $P\bar{1}$ (No. 2)
T	85(2) K	85(2) K
a	17.68230(10) Å	16.5646(2) Å
b	17.68230(10) Å	22.6005(3) Å
c	31.3310(2) Å	26.6734(3) Å
α	90°	85.5920(10)°
β	90°	72.7190(10)°
γ	90°	84.4050(10)°
Volume	9796.07(13) Å^3	9477.4(2) Å^3
λ	1.54178 Å	1.54178 Å
ρ_{calc}	1.286 g/cm^3	1.705 g/cm^3
Z	2	1
μ	11.169 mm^{-1}	16.769 mm^{-1}
F(000)	3692	4729
range	2.821° to 69.345°	1.737° to 69.884°
Limiting Indices	$-21<h<20$	$-20<h<20$
	$-21<k<21$	$-26<k<27$
	$-37<l<38$	$-31<l<32$
Reflections collected/unique	76333/4675	145338/34374
Completeness to θ	100.0%	97.9%
No. of Data/Restraints/Params	4675/978/428	34374/584/2375
GooF on F^2	1.085	1.028
[a]R_1	0.0619 [$I>2\sigma(I)$]; 0.0620 [all data]	0.0530 [$I>2\sigma(I)$]; 0.556 [all data]
[b]wR_2	0.1815 [$I>2\sigma(I)$]; 0.1816 [all data]	0.1419 [$I>2\sigma(I)$]; 0.1527 [all data]
Largest Diff. Peak, Hole	1.093 e·Å^{-3}, -1.022 e·Å^{-3}	3.266 e·Å^{-3}, -3.506 e·Å^{-3}

[a] $R_1 = \Sigma(||F_o|-|F_c||)/\Sigma|F_o|$

[b] $wR_2 = [\Sigma[w(F_o^2 - F_c^2)^2]/\Sigma[w(F_o)^2]]^{1/2}$; $w = 1/[\sigma^2(F_o^2) + (mp)^2 + np]$; $p = [\max(F_o^2,0) + 2F_c^2]/3$ (m and n are constants); $\sigma = [\Sigma[w(F_o^2 - F_c^2)^2/(n-p)]^{1/2}$

Photophysical Measurements

Luminescence data were collected on samples in the solid state and on freshly prepared 50 μM solutions in DMF placed in 2.4 mm i.d. quartz capillaries. Steady-state emission and excitation spectra were measured on a custom-designed Horiba Scientific Fluorolog 3 spectrofluorimeter equipped with either a visible photomultiplier tube (PMT) (220-850 nm, R928P; Hamamatsu) or a NIR PMT (950-1650 nm, H10330-75; Hamamatsu) upon excitation with a continuous Xenon lamp. Time-resolved phosphorescence spectra of **Gd-I$_x$** MCs (x = 0, 4, 8, 12) in the solid state were acquired at 77 K upon excitation with a flash Xenon lamp and applying a time delay (Figure S 15). All excitation and emission spectra were corrected for the instrumental functions. Luminescence lifetimes (τ_{obs}) were determined under excitation at 355 nm provided by a Nd:YAG laser (YG 980; Quantel). Signals were detected in the visible or NIR ranges using an iHR320 monochromator (Horiba Scientific) equipped with a Hamamatsu R928P and H10330-75 PMTs. The output signal from the detector was fed into a 500 MHz bandpass digital oscilloscope (TDS 754C; Tektronix), transferred to a PC for data processing with the program Origin 8®. Luminescence lifetimes are averages of at least three independent measurements. Yb^{3+}-centered quantum yields under ligands excitation (Q_{Yb}^{L}) at 320–350 nm were determined with the Fluorolog 3 spectrofluorimeter based on an absolute method with the use of an integration sphere (Model G8, GMP SA, Renens, Switzerland). Each sample was measured several times under comparable experimental conditions, varying the position of samples. Estimated experimental error for quantum yield determination is ~10 %.

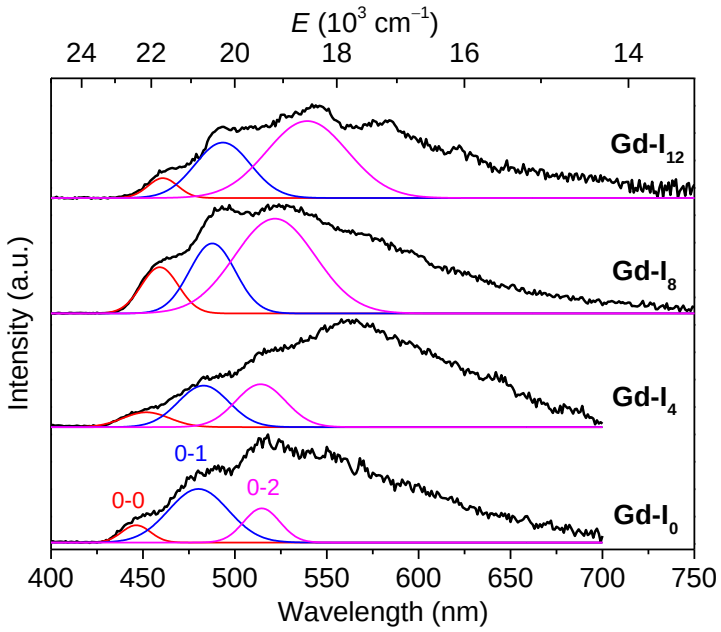

Figure S 15. Corrected and normalized phosphorescence spectra (black traces) of **Gd-I$_x$** MCs (x = 0, 4, 8, 12) in the solid state (λ_{ex} = 320–340 nm, time delay after the excitation flash 100 µs, 77 K). 0–0, 0–1 and 0–2 phonon transitions (colored traces) were fitted with Gaussian function.

Table S2. Energies of 0-0, 0-1 and 0-2 phonon transitions in the phosphorescence spectra of **Gd-I$_x$** MCs (x = 0, 4, 8, 12) in the solid state at 77K (Figure S15).

Gd-I$_x$	E (cm^{-1})					
	0-0	0-1	0-2	$\Delta_{0\text{-}1}$	$\Delta_{1\text{-}2}$	Δ_{av}[a]
Gd-I$_0$	22385	20890	19435	1495	1455	1475(30)
Gd-I$_4$	22130	20705	19450	1425	1255	1340(125)
Gd-I$_8$	21780	20490	19230	1290	1260	1275(50)
Gd-I$_{12}$	21730	20100	18590	1630	1510	1570(90)

[a] Standard deviation values between parentheses.

Table S3. Observed (τ_{obs}) and radiative (τ_{rad}) lifetimes, intrinsic ($\boldsymbol{Q_{Yb}^{Yb}}$) and total ($\boldsymbol{Q_{Yb}^{L}}$) quantum yields, and sensitization efficiencies (η_{sens}) of **Yb-I*x*** (x = 0, 4, 8, 12) in the solid state at room temperature.[a]

Yb-I*x*	τ_{obs} (μs)[b]	τ_{rad} (μs)[c]	Q_{Yb}^{Yb} (%)[d]	Q_{Yb}^{L} (%)[e]	η_{sens} (%)[f]
Yb-I$_0$	37.1(1)	270	14	4.82(4)	35
Yb-I$_4$	22.4(1)	210	11	1.45(5)	13.6
Yb-I$_8$	22.4(5)	250	9.0	1.17(1)	13.0
Yb-I$_{12}$	13.6(1)	150	8.8	0.78(2)	8.9

[a] 2σ values within parentheses. Relative errors: τ_{obs}, ±2%; Q_{Yb}^{L} , ±10 %; τ_{rad}, ±10%; Q_{Yb}^{Yb} , ±12 %; η_{sens}, ±22 %. [b] λ_{ex} = 355 nm. [c] Recalculated from values in DMF solutions assuming n = 1.5. [d] From eq. (1) and (S2). [e] λ_{ex} = 330 nm for **Yb-I$_0$**, **Yb-I**$_4$, or 350 nm for **Yb-I$_8$**, **Yb-I$_{12}$**. [f] From eq. (1) and (S3).

Photostability Studies

For practical optical imaging applications, photostabilities of the probes are important parameters that characterize their ability to be used for quantitative, long-term or repeated experiments. Therefore, we have studied changes in emission intensities at 980 nm of solutions of **Yb-I$_x$** (x = 0, 4) and **Yb-I$_x$** (x = 8, 12) upon continuous illumination at 320 or 335 nm (power ~25 mW cm^{-2}), respectively, during > 2 h (Figure S16). After photobleaching experiments excitation and emission spectra were acquired and compared to the initial ones (Figure S17). It was found that the NIR Yb^{3+} emission intensity of the **Yb-I$_0$** MC observed at 980 nm decreases almost linearly down to 60 % after 2h of illumination. The iodination induces significant changes in the behavior at the beginning of the illumination time, but after 30, 40 or 60 min for **Yb-I$_4$**, **Yb-I$_8$** and **Yb-I$_{12}$**, respectively, a linear dependence of the NIR emission decrease is recovered. Such results could reflect a chemical modification of iodinated salicylhydroximate and/or isophthalate ligands upon illumination, i.e. release of iodine. Indeed, for **Yb-I$_8$** and **Yb-I$_{12}$,** a discoloration of the solutions after experiments was observed along with a significant blue shift of the excitation band (Figure S 17). In addition, changes in absorption spectra were noted for **Yb-I$_8$** and **Yb-I$_{12}$** during irradiation with 365 nm light (Figures S18, S19). Mass spectrometry analysis of the resulting solutions after photobleaching experiments confirmed the loss of iodide (Figure S20). Therefore, two main processes are acting in parallel upon illumination of **Yb-I$_x$**: photobleaching and release of iodine. In this case, an increase of the emission intensity for **Yb-I$_8$** and **Yb-I$_{12}$** upon illumination can be explained by the formation of significantly more luminescent **Yb-I$_0$** species in solution (Table 1, main text). It should be noted that photobleaching experiments for **Yb-I$_x$** were repeated three times and the same behavior (within experimental uncertainties) was observed.

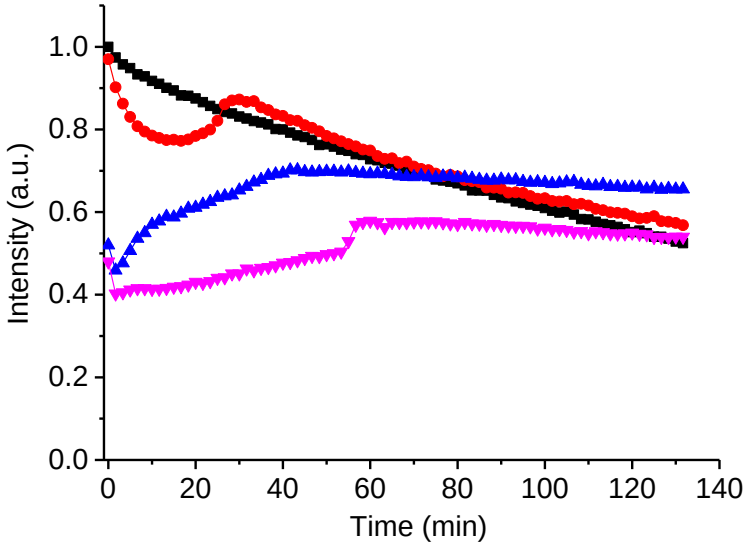

Figure S 16. Changes in emission intensities at 980 nm for **Yb-I$_x$** MCs upon continuous illumination at 320 nm (x = 0, 4) or 335 nm (x = 8, 12) (50 µM, DMF, room temperature). Black : **Yb-I$_0$** ; red : **Yb-I$_4$** ; blue : **Yb-I$_8$** ; magenta : **Yb-I$_{12}$**. For the sake of comparison, the intensity at *Time* = 0 min for the **Yb-I$_0$** is normalized to 1, while the others were scaled according to the quantum yield values, i.e. 0.97 for **Yb-I$_4$** , 0.52 for **Yb-I$_8$** and 0.48 for **Yb-I$_{12}$**.

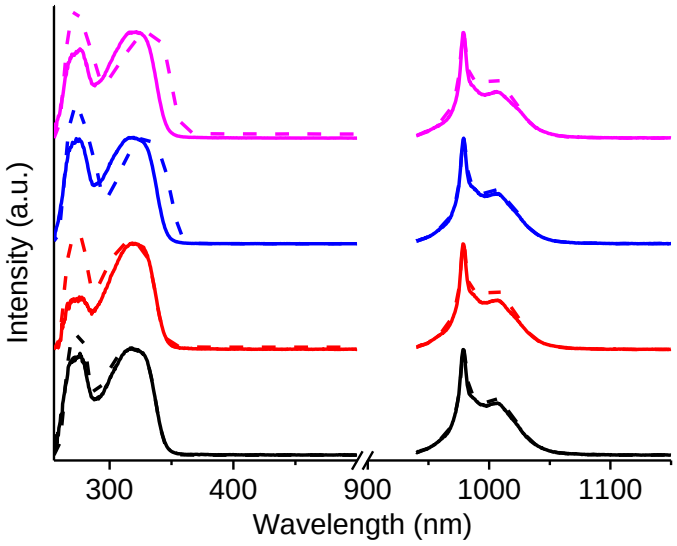

Figure S 17. Comparison between normalized (left) excitation (λ_{em} = 980 nm) and (right) emission (λ_{ex} = 320 or 335 nm) spectra of **Yb-I$_x$** MCs (x = 0, 4, 8, 12) before (dashed traces) and after (solid traces) photobleaching experiments (50 µM, DMF, room temperature). For the sake of comparison, excitation spectra are normalized on the maximum of the low-energy band while emission spectra were normalized to the band at 980 nm. Black : **Yb-I$_0$** ; red : **Yb-I$_4$** ; blue : **Yb-I$_8$** ; magenta : **Yb-I$_{12}$**.

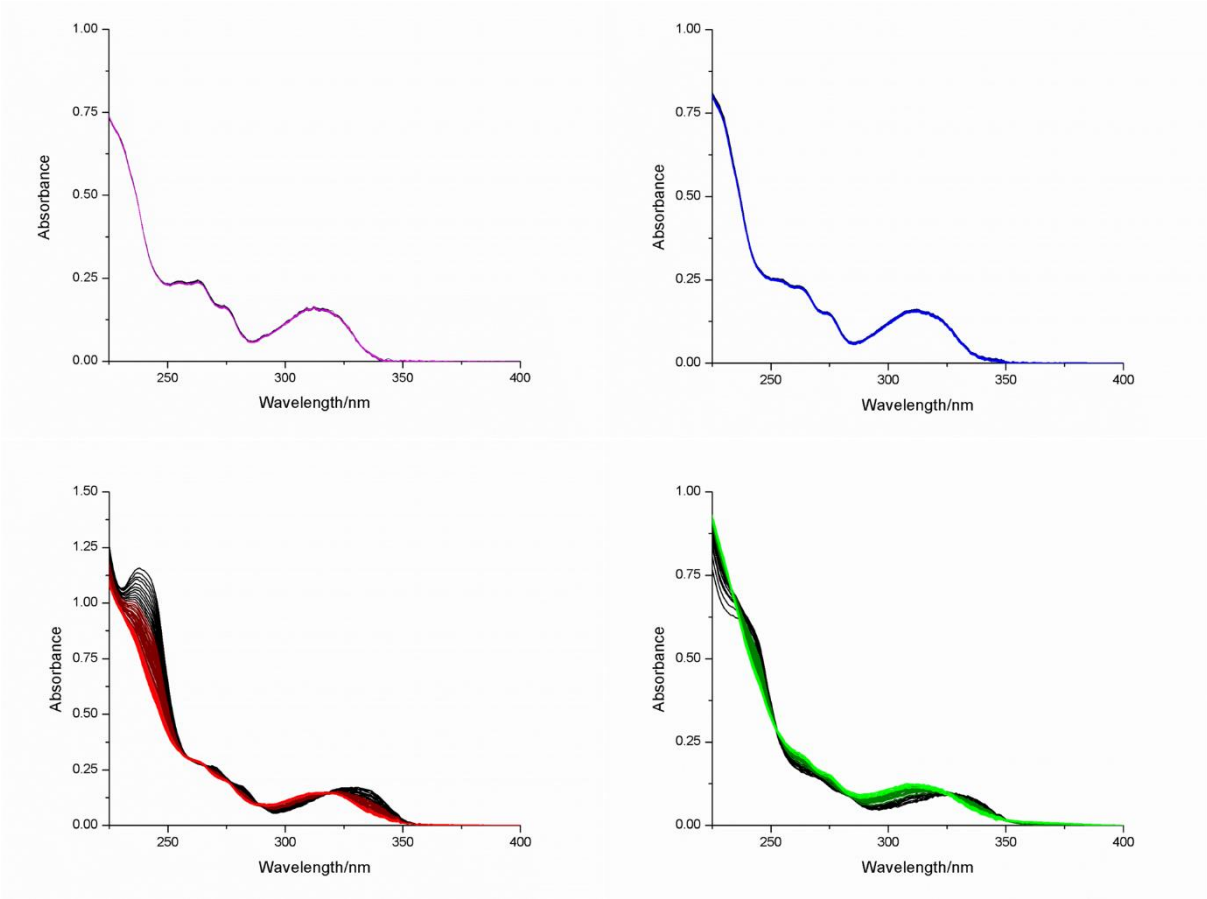

Figure S 18. Overlay of UV–Vis spectra of **Yb-I$_0$** (purple, top left), **Yb-I$_4$** (blue, top right), **Yb-I$_8$** (red, bottom left) and **Yb-I$_{12}$** (green, bottom right) in methanol (2–5 µM) recorded every 5 minutes over the course of three hours while irradiating with 365 nm excitation light. Measurements were performed on a Cary 100Bio UV–Vis spectrophotometer.

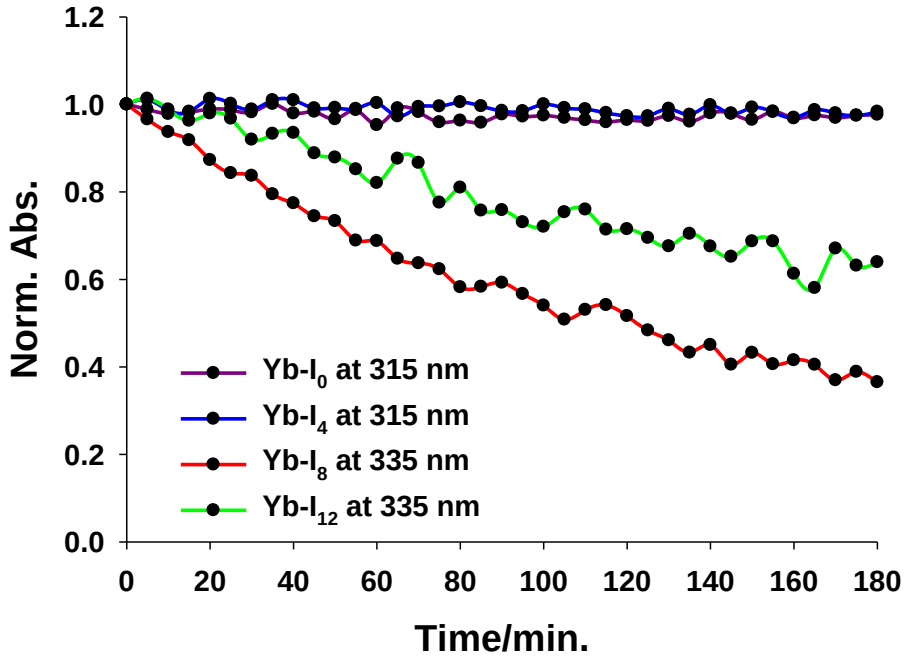

Figure S 19. Normalized absorbance values collected over time for each **Yb-I$_x$** species shows a change in absorbance for x = 8 and x = 12.

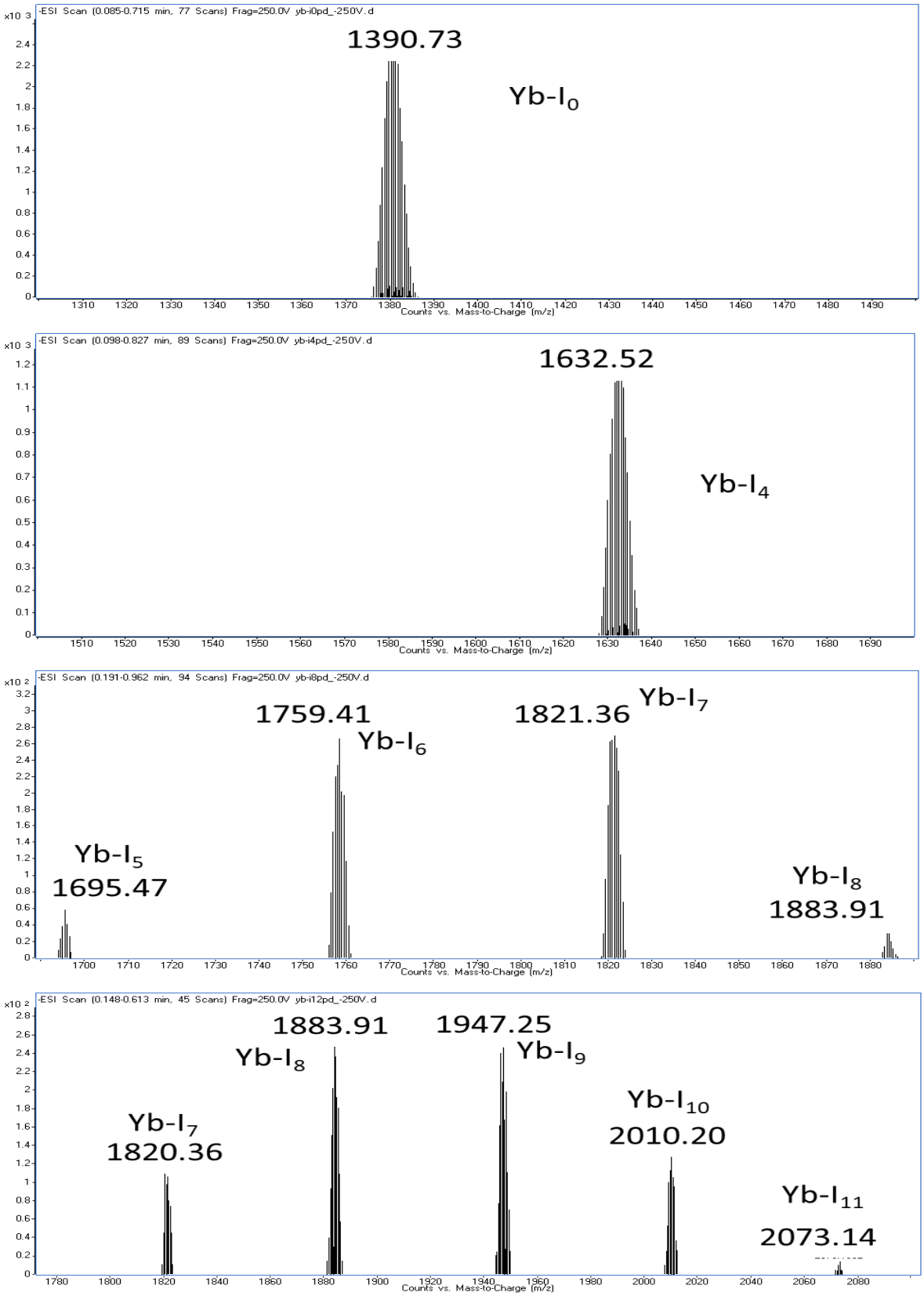

Figure S 20. ESI-MS spectra of methanol solutions of **Yb-I$_x$** MCs collected after 6 hours irradiation with the 365 nm light. **Yb-I$_8$** fragments into x = 5 to 8 and **Yb-I$_{12}$** fragments into x =7 to 11. **Yb-I$_0$** and **Yb-I$_4$** do not change.

Determination of Yb^{3+} radiative lifetimes

Absorption spectra in the UV-visible-NIR range were collected on 50 µM, 0.5 or 5 mM solutions of **Yb-I$_x$** (x = 0, 4, 8, 12) in DMF using a Jasco V670 UV-Vis-NIR spectrophotometer in absorbance mode.

Yb^{3+} radiative lifetimes (τ_{rad}) were determined from the absorption spectra in the range of the $^2F_{5/2} \leftarrow {}^2F_{7/2}$ transition (Figure S 21) using a modified Einstein's equation:

$$\frac{1}{\tau_{rad}} = 2303 \times \frac{8\pi c n^2 \tilde{\nu}_m^2 (2J+1)}{N_A (2J'+1)} \int \varepsilon(\tilde{\nu}) d\tilde{\nu} \qquad \text{(S1a)}$$

$$\tilde{\nu}_m = \frac{\int \tilde{\nu} \varepsilon(\tilde{\nu}) d\tilde{\nu}}{\int \varepsilon(\tilde{\nu}) d\tilde{\nu}} \qquad \text{(S1b)}$$

where c is the speed of light in centimeters per second, n is refractive index (n_{DMF} = 1.43), N_A is the Avogadro's number, J and J' are the quantum numbers for the ground and excited states, respectively, $\int \varepsilon(\tilde{\nu}) d\tilde{\nu}$ is the integrated spectrum of the f-f transition, $\tilde{\nu}_m$ is the barycenter of the transition.

Intrinsic quantum yields (Q_{Yb}^{Yb}) and sensitization efficiencies (η_{sens}) were calculated using the following equations:

$$Q_{Yb}^{Yb} = \frac{\tau_{obs}}{\tau_{rad}} \times 100\% \qquad \text{(S2)}$$

$$\eta_{sens} = \frac{Q_{Yb}^{L}}{Q_{Yb}^{Yb}} \times 100\% \qquad \text{(S3)}$$

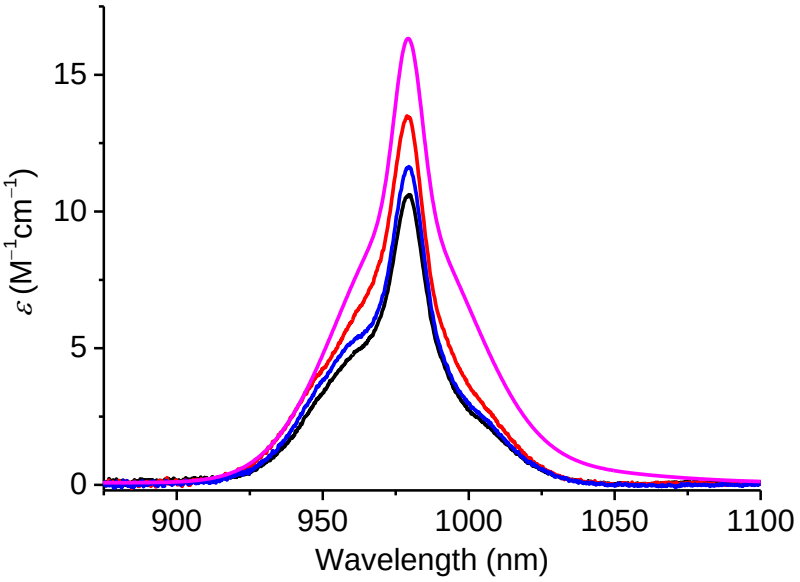

Figure S 21. Absorption spectra of **Yb-I*x*** recorded in the range of the $^2F_{5/2} \leftarrow ^2F_{7/2}$ transition (DMF, 5 mM for x = 0, 4, 8 or 0.5 mM for x = 12) at 293 K. Black : **Yb-I$_0$** ; red : **Yb-I$_4$** ; blue : **Yb-I$_8$** ; magenta : **Yb-I$_{12}$**.

X-ray Computed Tomography and Attenuation Measurements

The comparative radiodensity investigations of **Yb-I$_x$** (x = 0, 4, 8, 12) were performed using a Bruker Skyscan 1278 with the following CT-scan parameters: 45 kV and 996 µA (RTW MCB 65M tube, tungsten anticathode). The scanner was used in a 'soft tissue' mode to get around 20-30% of X-ray transmission for the most concentrated samples. A number of 4 projections were averaged per quarter of angle along the 360° of scan around the samples. The voxel resolution was 103.562×103.562×103.562 µm.

For XCT experiments, a serial dilution of the stock 20 mM solution of **Yb-I$_x$** (x = 0, 4, 8, 12) in DMF was prepared in a conical bottom 96 well plate devoted to qPCR experiments. As a result, the wells were filled with 40 µL of 20 mM, 10 mM, 5 mM, 2.5 mM, 1.25 mM, 625 µM or 80 µL of 312.5 µM solutions of **Yb-I$_x$** (x = 0, 4, 8, 12) in DMF. For quantification and determination of attenuations, expressed in Hounsfield Units (*HU*), reference wells filled with water were used and set at 0 *HU*, whereas the ones filled with air was set at -1000 *HU*. Since DMF is less dense than water, its attenuation was subtracted from all values, as a blank, to consider only the attenuation induced by the **Yb-I$_x$** (x = 0, 4, 8, 12) metallacrowns without the contribution of the solvent. The molar X-ray attenuation coefficient (HU_m) was determined with the help of the following formula:

$$HU_m = \frac{HU}{VOI[L] \times c\left[\frac{mol}{L}\right]},$$

where *VOI* is the volume of interest defined as :

$$VOI[L] = N_{voxel} \times V_{voxel}[L].$$

As a reference, a commercially available solution of Xenetix (Iobitridol) in water at 548.4 mg/mL (corresponding to an iodine concentration of 250 mg/mL) was used and its molar X-ray attenuation coefficient was quantified as described above.

References

(1) Fischer, E.; Speier, A. Darstellung Der Ester. *Berichte der Dtsch. Chem. Gesellschaft* **1895**, *28* (3), 3252–3258. https://doi.org/10.1002/cber.189502803176.

(2) Bazaga-García, M.; Colodrero, R. M. P.; Papadaki, M.; Garczarek, P.; Zoń, J.; Olivera-Pastor, P.; Losilla, E. R.; León-Reina, L.; Aranda, M. A. G.; Choquesillo-Lazarte, D.; et al. Guest Molecule-Responsive Functional Calcium Phosphonate Frameworks for Tuned Proton Conductivity. *J. Am. Chem. Soc.* **2014**, *136* (15), 5731–5739. https://doi.org/10.1021/ja500356z.

(3) Sheldrick, G. M. Crystal Structure Refinement with SHELXL. *Acta Crystallogr. Sect. C Struct. Chem.* **2015**, *71* (1), 3–8. https://doi.org/10.1107/S2053229614024218.

(4) Spek, A. L. Single-Crystal Structure Validation with the Program PLATON. *J. Appl. Crystallgraphy* **2003**, *36*, 7–13. https://doi.org/10.1107/S0021889802022112.

(5) Spek, A. L. PLATON SQUEEZE: A Tool for the Calculation of the Disordered Solvent Contribution to the Calculated Structure Factors. *Acta Crystallogr. Sect. C Struct. Chem.* **2015**, *71* (1), 9–18. https://doi.org/10.1107/S2053229614024929.

(6) Nguyen, T. N.; Chow, C. Y.; Eliseeva, S. V.; Trivedi, E. R.; Kampf, J. W.; Martinić, I.; Petoud, S.; Pecoraro, V. L. One-Step Assembly of Visible and Near-Infrared Emitting Metallacrown Dimers Using a Bifunctional Linker. *Chem. - A Eur. J.* **2018**, *24* (5), 1031–1035. https://doi.org/10.1002/chem.201703911.

(7) Wang, J.; Lu, G.; Liu, Y.; Wu, S.; Huang, G.; Liu, J.; Tong, M. Building Block and Directional Bonding Approaches for the Synthesis of {DyMn4}n (n = 2, 3) Metallacrown Assemblies. *Cryst. Growth Des.* **2019**, *19*, 1896–1902. https://doi.org/10.1021/acs.cgd.8b01879.

(8) Pecoraro, V. L.; Stemmler, A. J.; Gibney, B. R.; Bodwin, J. J.; Wang, H.; Kampf, J. W.; Barwinski, A. Metallacrowns: A New Class of Molecular Recognition Agents. In *Progress in Inorganic Chemistry, Volume 90*; Karlin, K. D., Ed.; John Wiley & Sons, Inc., 1997; pp 83–178. https://doi.org/10.1002/9780470166468.ch2.